FEBS Letters 585 (2011) 2205–2211

FEBS Letters

journal homepage: www.FEBSLetters.org

A role for myelin-associated peroxisomes in maintaining paranodal loops and axonal integrity

Celia M. Kassmann [a], Susanne Quintes [a], Jens Rietdorf [b], Wiebke Möbius [a], Michael Werner Sereda [a], Tobias Nientiedt [a], Gesine Saher [a], Myriam Baes [c], Klaus-Armin Nave [a,*]

[a] Department of Neurogenetics, Max Planck Institute of Experimental Medicine, Hermann-Rein-Str. 3, D-37075 Göttingen, Germany
[b] Friedrich Miescher Institute, Basel, Switzerland
[c] Laboratory of Cell Metabolism, K.U. Leuven, Leuven, Belgium

ARTICLE INFO

Article history:
Received 4 October 2010
Revised 11 May 2011
Accepted 12 May 2011
Available online 23 May 2011

Edited by Wilhelm Just

Keywords:
Myelin
Peroxisome
PEX5
Adrenoleukodystrophy
Energy-metabolism

ABSTRACT

Demyelinating diseases of the nervous system cause axon loss but the underlying mechanisms are not well understood. Here we show by confocal and electron microscopy that in myelin-forming glia peroxisomes are associated with myelin membranes. When peroxisome biogenesis is experimentally perturbed in Pex5 conditional mouse mutants, myelination by Schwann cells appears initially normal. However, in nerves of older mice paranodal loops become physically unstable and develop swellings filled with vesicles and electron-dense material. This novel model of a demyelinating neuropathy demonstrates that peroxisomes serve an important function in the peripheral myelin compartment, required for long-term axonal integrity.

1. Introduction

Myelin provides the physical basis for saltatory impulse propagation in the nervous system [1]. However, there are additional functions of myelinating glia in the maintenance of axonal integrity that are independent of myelin itself [2–4]. This supportive role of glia is reflected in the clinical phenotype of myelin diseases with secondary axon loss, such as in demyelinating neuropathies [5,6]. The mechanisms by which glial cells support axon function is not understood, but may have a metabolic component [7].

Peroxisomes are ubiquitous organelles in eucaryotic cells [8]. They provide small subcellular compartments for oxidative metabolic reactions, including β-oxidation of fatty acids, branched chain fatty acids, eicosanoids and a oxidation of 2-hydroxy fatty acids. Peroxisomal catalase detoxifies hydrogen peroxide, generated as a side product of these reactions, thereby reducing oxidative stress [9]. Peroxisomes are also involved in the synthesis of plasmalogens, a class of etherphospholipids that have an anti-oxidant function [10].

An important role for peroxisomes in the nervous system is suggested by several metabolic diseases in which some or all peroxisomal functions are lost. X-linked adrenoleukodystrophy (X-ALD) and Refsum's disease are two such neurodegenerative diseases. Lethal developmental disorders also include Zellweger syndrome and neonatal adrenoleukodystrophy [11].

In the brain, peroxisomes are detected in virtually all cell types and often differ in size [12,13]. To define the critical cell type of peroxisomal dysfunction in metabolic defects of the nervous system, PEX5-dependent peroxisome biogenesis was inactivated in single cell types. For oligodendrocytes, this resulted in the degeneration of myelinated axons but, remarkably, without affecting oligodendrocyte survival [14–16].

To better understand the relationship of peroxisomes in the neuronal and glial compartment, we analyzed their subcellular distribution by two-photon and confocal microscopy. Here we show that peroxisomes are highly abundant in myelinated fiber tracts, but largely contained in the glial compartment and rarely within axons. Ultrastructurally and biochemically, these peroxisomes are associated with non-compacted myelin membranes. To determine their function for myelin integrity, we analyzed Cnp-Cre*PEX5flox/flox mice that lack peroxisomes in the Schwann cell lineage. This study revealed that progressive myelin degeneration, with paranodal swellings and accumulations of electron-dense material, defines a novel gene defect with neuropathy in mice, and supports a model of glial metabolic support for axon function.

* Corresponding author. Fax: +49 551 3899 758.
E-mail address: nave@em.mpg.de (K.-A. Nave).

0014-5793/$36.00
doi:10.1016/j.febslet.2011.05.032

2. Materials and methods

2.1. Mouse genetics

Cnp1-Cre*PEX5flox/flox mice [14] were maintained in individually ventilated cages under SPF conditions. Animal experiments were carried out in compliance with approved animal policies of the MPI of Experimental Medicine.

2.2. Immunohistochemistry, immunohistology and fluorescent microscopy

For preparation of teased fibers 2 months old wildtype C57/bl6 mice were perfused with 10 ml HBSS followed by 10 ml of 4% PFA, 4% PFA in 30% sucrose or 30% sucrose solution. Sciatic nerves were dissected, transferred into PBS and immediately teased on a glass slide under a binocular using 20 gauge needles. After drying, slides were stored at −20 °C. Primary oligodendrocytes were prepared from newborn C57/bl6 mice and differentiated cells were fixed as described [3].

We used antibodies for histology as follows: ACAA1 (ProteinTech Group) 1:500; ACOX1 (ProteinTech Group) 1:200; Catalase (Rockland) 1:1000; CASPR (Neuromab) 1:1000; CNP (Sigma) 1:300; MAG (clone 513) 1:50 [17]; MBP monoclonal (Covance) 1:1000; MFP1 (S78) 1:2000, kindly provided by W. Just, Heidelberg; neurofilament (FNP7; Zymed) 1:200; neurofilament (NF200; Sigma) 1:100; PEX14 (ProteinTech Group) 1:100; PLP (clone O10) [18] 1:50; PMP-70 (Abcam) 1:500. Fluorescently labeled secondary antibodies were used as follows: Cy2 (Jackson ImmunoResearch) 1:200; Cy3 (Jackson ImmunoResearch) 1:2000. Nuclear staining dye: ToPro-3 (Invitrogen) 1:1000.

Fluorescence light microscopy was carried out with a confocal laser-scanning microscope (LSM 510, Axiovert 200, Zeiss). To detect Cy2 samples were excited at 488 nm and detected through a 500–550 nm bandpass filter. Cy3 was excited at 543 nm and detected with a 565–615 nm bandpass filter. All confocal images were processed with ImageJ software. For two-photon confocal microscopy data volumes sampled at Nyquist rate were acquired on a commercial two-photon setup SP5R MP (Leica, Mannheim) equipped with a 1.1 NA glycerol immersion objective and a tunable pulsed laser set to 930 nm.

For demonstrating colocalization, two-photon images dual channel data volumes were analyzed using the 'spot-finder' functionality of the commercial software Imaris (Bitplane AG, Switzerland). Objects were automatically identified in the channel representing labeled peroxisomes (green false color). In a volume of 0.06 μm^3 around the center coordinate of each object, average intensities were measured in the channel representing the myelin (red false color). Then, using the same data volumes, an equal number of random objects was created and intensities were measured as described above. The intensities measured for each condition were sorted and submitted to Mann–Whitney *U-test ("R" software).*

2.3. Muscle histology

Cryostate tissue sections of m. soleus and m. gastrocnemius (14 μm) were analyzed directly for Evans blue derived fluorescence or processed for H&E and myosin ATPase (pH 4.3) histochemistry according to standard procedures.

2.4. Electron microscopy

Transmission and immuno-electron microscopy was carried out as previously described [19]. For immuno-labeling, sections were incubated with polyclonal rabbit antibodies specific for catalase (Rockland) and PMP70 (Abcam), and antigens visualized with protein A-gold (10 nm or 15 nm). Embedding of teased fibers for electronmicroscopy followed the dissection of sciatic nerves from animals that had been fixed by transcardial perfusion with 4% PFA and 2.5% glutar-di-aldehyde in 0.2 M phosphate buffer. Nerves were postfixed in 2% osmiumtetroxide at 4 °C for 2 h. The perineurium was removed under a binocular and the nerves were pre-teased into fiber bundles. The following steps were carried out in plastic tubes on an overhead rotator. Bundles were dehydrated via a graded series of alcohol (30%, 50%, 70%, 90%, 99.9% ethanol, 15 min each) followed by a 15 min incubation in propylenoxide. After infiltration of bundles by mixtures of propylenoxide/epoxy resin (2:1, 1:1, 1:2, 30 min each), specimens were kept rotating in epoxy resin for at least 2 h. Finally, bundles were placed into a drop of resin on a glass slide and teased into single fibers. A resin-filled gelatine capsule was put on top of the fibers and polymerized at 60 °C for 24 h. Ultrathin sections (5080 nm) were cut and counterstained with uranyl acetate and Reynold's lead citrate.

2.5. Protein biochemistry

Myelin membranes were enriched from total brain lysates by a modified procedure of Norton and Poduslo [19], which included two rounds of sucrose step gradient (0.85 M/0.32 M) centrifugation with an intervening osmotic shock. Protein content was measured using Bradford essay (Biorad) according to the manufacturer's instruction. For Western blots we used antibody concentrations and protein amounts as follows: ACAA1 (ProteinTech Group) 1:500, 25 μg loaded; Catalase (Rockland) 1:1000; Actin (Chemicon) 1:1000, 10μg μg loaded; MFP1 (S78) 1:2000 kindly provided by W. Just, Heidelberg, 15 μg loaded; PEX14 (ProteinTech Group) 1:100, 20 μg loaded; PLP (clone 3F4) 1:50, kindly provided by M. Lees, 2 μg of myelin fractions, 10 μg of total brain lysates; PMP-70 (Abcam) 1:1000, 15 μg loaded; PEX5 (BD Biosciences) 1:200, 10 μg loaded.

2.6. Electrophysiology

Electrophysiology was performed for sciatic nerves at the age 2, 6 and 9 months. Mice were anaesthetized with ketaminhydrochloride (100 mg kg^{-1})/xylazin hydrochloride (8 mg kg^{-1}). A pair of steel needle electrodes was placed subcutaneously along the nerve at sciatic notch (proximal stimulation). A second pair of electrodes was placed along the tibial nerve above the ankle (distal stimulation). Supramaximal square wave pulses lasting 100 ms were delivered using a Toennies Neuroscreen® (Jaeger, Hoechsberg, Germany). Compound muscle action potential (CMAP) was recorded from the intrinsic foot muscles. Both amplitudes and latencies of CMAP were determined. The distance between the two sites of stimulation was measured alongside the skin surface with fully extended legs and nerve conduction velocities (NCVs) were calculated from sciatic nerve latency measurements.

3. Results

3.1. Most peroxisomes in white matter are associated with glia, not axons

To determine the localization of peroxisomes in myelinated fiber tracts we first studied the subcortical white matter, in which peroxisomal disorders cause the most severe pathology. For confocal identification, we used antibodies against peroxisomal membrane protein 70 (PMP70) or catalase. Axons were visualized with antibodies against neurofilament light chain (FNP7), and oligodendrocytes and myelin were stained for myelin basic protein or CNPase.

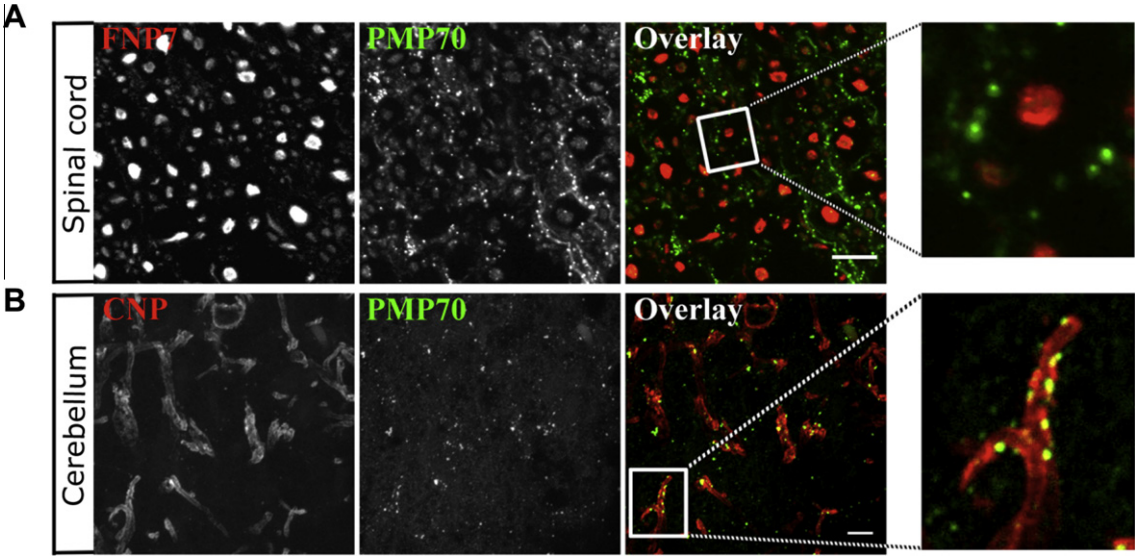

Fig. 1. Myelin-associated peroxisomes in the CNS. (A) Dorsal columns of the cervical spinal cord (age 2 months). Confocal image showing myelinated axons in cross-section (neurofilament/FNP7, in red) and glial peroxisomal puncta (PMP70, in green) that are arranged around axons but not colocalizing (magnified to the right). (A) Cerebral white matter. Maximal intensity projection (volume $100 \times 100 \times 15\ \mu m^3$) of a two-photon confocal image of myelin sheaths (CNP, in red) and peroxisomal puncta that colocalize with myelin (PMP-70, in green). Scale bars 10 μm.

In cultured neurons, peroxisomes are readily found in the axonal compartment [20]. Surprisingly, in the corpus callosum of adult wildtype mice, the majority of peroxisomes were associated with oligodendrocytes and the myelin sheath, but not with axons (Suppl. Video 1). To investigate this phenomenon in more detail, we studied the spinal cord, in which axon myelin units are considerably larger. Also here, peroxisomes generally decorated individual axons (Suppl. Video 2). In cross-sections of the dorsal columns PMP70-stained peroxisomes were distributed in between FNP7-positive axons (Fig. 1A). Some peroxisomes appeared associated with the abaxonal aspect of the sheath, separated by a ring of unstained myelin (Fig. 1A). In overlays, only very few puncta appeared within axons (not shown). In the cerebellar white matter, there was extensive colocalization of peroxisomes with CNP-labeled myelin profiles (Fig. 1B), which was highly significant ($P < 0.005$) when quantified (data not shown).

To better define the subcellular localization of peroxisomes, we analyzed primary oligodendrocytes in a monolayer culture. When

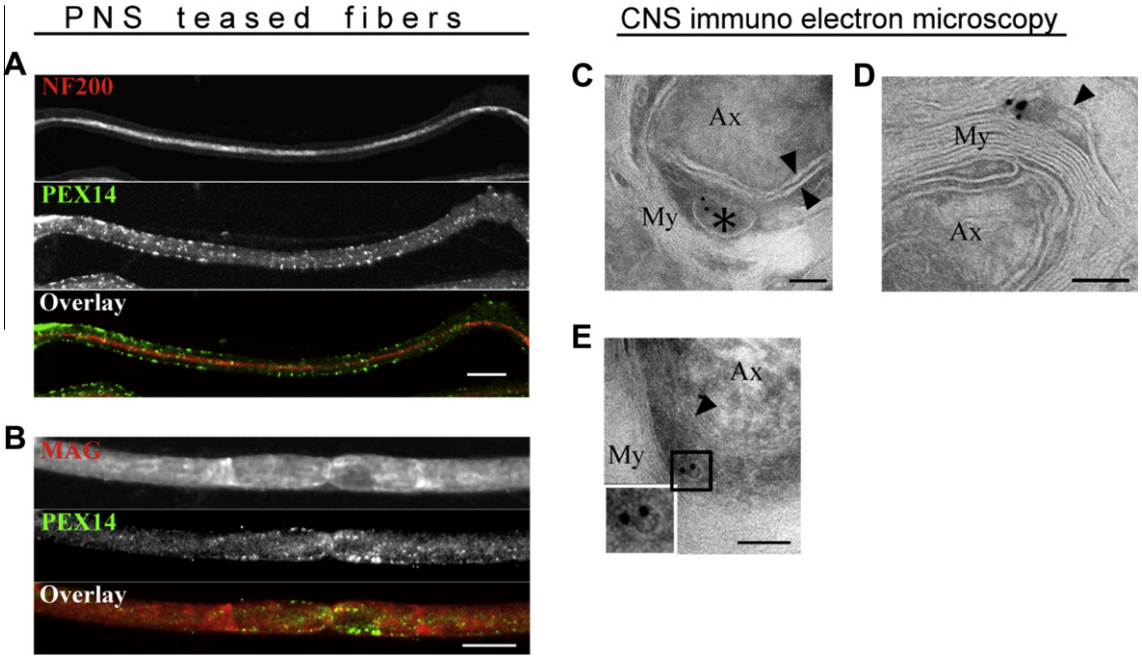

Fig. 2. Peroxisomes in the inner and outer mesaxon of myelinating glia. (A) Confocal analysis of teased fibers from adult sciatic nerves. Most peroxisomal puncta (PEX14, in green) are associated with the outer aspect of the myelinated axon (stained for neurofilament/NF200 in red). (B) In peripheral nerves, peroxisomal puncta (PEX14, in green) colocalize with myelin (MAG, in red). Scale bars 15 μm. (C) In corpus callosum of adult mice, immuno-electron microscopy confirms the localization of peroxisomes in non-compacted myelin. Immunogold-labeling of catalase identifies a single peroxisome (asterisk) in the inner mesaxon of a callosal fiber. Arrowheads indicate axonal and innermost oligodendroglial membranes. (D) PMP-70 (PAG-15) and catalase (PAG-10) double-positive peroxisomes were also found in the outer mesaxon of myelinated spinal cord axons. (E) 'Microperoxisome' in the inner mesaxon of a myelinated, immuno-labeled for catalase. Note the small size of this peroxisome (about 30 nm) as magnified in inset. My, myelin; Ax, axon. Scale bars 100 nm.

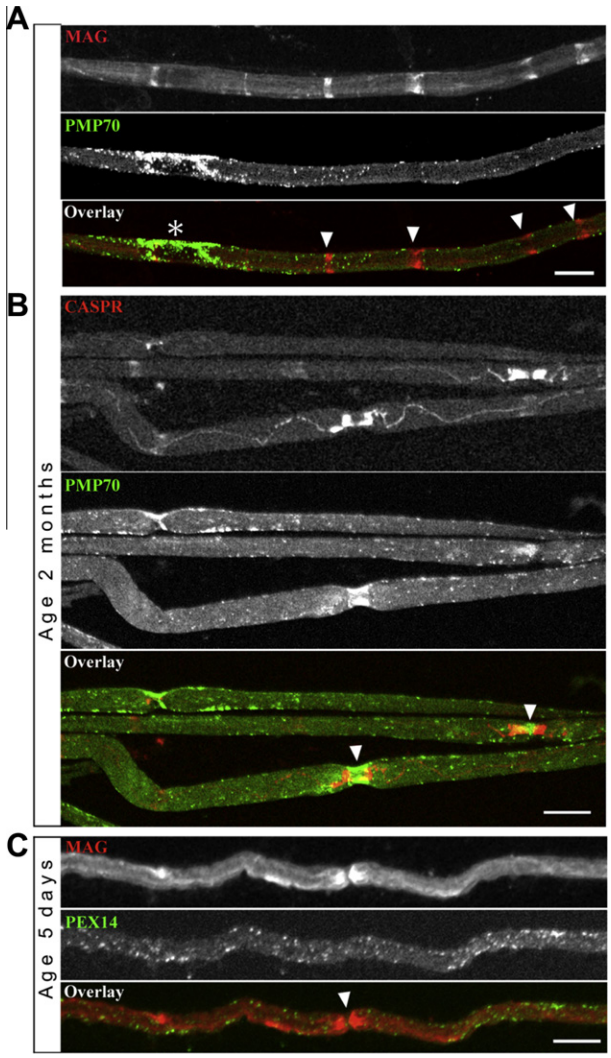

Fig. 3. Subcellular localization of peroxisomes in teased PNS fiber preparations. (A) In myelinating Schwann cells, PMP70-positive peroxisomes (middle) reside close to the cell nucleus (asterisk) and are associated with myelin, but not with MAG positive Schmidt-Lantermann incisures (top). Scale bar 15 μm. (B) PMP70-positive peroxisomes (in green) reside in paranodal loops (arrowhead), identified by their close proximity to the axonal marker Caspr (in red). Scale bar 15 μm. (C) At early myelinating stages (P5), glial peroxisomes are dispersed along the internode (PEX14 in green), but not (yet) in the MAG-stained paranodal region (red, arrowhead), suggesting that peroxisomes are transported after myelination. Scale bar 10 μm.

double-stained for myelin basic protein (MBP) and PMP70 (or PEX14), peroxisomes appeared abundant in mature oligodendrocytes with extended membrane sheets (Suppl. Fig. 1A and B). Acyl-CoA oxidase 1 (ACOX1), multifunctional protein 1 (MFP1) and catalase were readily visualized in oligodendroglial peroxisomes (Suppl. Fig. 1C–E). While the highest density of puncta was found in the perinuclear region, peroxisomes were also found in branched processes between large membrane sheets (Suppl. Fig. 1A–E).

In longitudinal sections of the spinal cord, the density of oligodendroglial peroxisomes was highest in the cell soma [21]. This observation was confirmed in brain sections detecting different peroxisomal membrane (PEX14, ABCD1, PMP70) and matrix proteins (ACOX1, MFP1, MFP2, ACAA1; catalase; data not shown).

3.2. Peroxisomes are associated with myelin

We confirmed the association of peroxisomes with oligodendrocyte processes and myelin at the biochemical level by studying purified myelin membranes (Suppl. Fig. 2). By Western blotting (Suppl. Fig. 2A and B), the integral membrane protein PMP70 was found in myelin as well as in whole brain lysates, demonstrating that the enrichment of myelin does not completely deplete peroxisomes. The observation that peroxisomal matrix proteins, including acyl-CoA oxidase (ACOX1), multifunctional proteins (MFP1 and MFP2), and acyl-CoA acetyltransferase (ACAA1) were lacking from the myelin fraction (Suppl. Fig. 2A) may be due to the purification method involving an osmotic shock. Why catalase was abundant in myelin is not clear, and we cannot rule out that myelin-associated peroxisomes have a higher catalase content. We also noted a band of lower mobility in myelin, the abundance of which was antibody-dependent, possibly by cross-reactivity.

We hypothesized that the principle relationship between glial peroxisomes and myelin is the same in oligodendrocytes and Schwann cells. Because myelinated axons are easier to study in peripheral nerves, we prepared teased fibers from the sciatic nerves of adult mice and immuno-labeled axons and myelin with antibodies against NF200 and myelin associated glycoprotein (MAG), respectively. Peroxisomes were identified with antibodies against PEX14, PMP70 and catalase and almost exclusively 'outside' the axon (Fig. 2A), similar to our findings in the CNS. Many puncta were seen at the edge of myelinated fibers, presumably in Cajal bands (Suppl. Video 3). MAG staining overlapped with peroxisomal markers (Fig. 2B), and allowed visualization of some peroxisomes at the adaxonal surface of myelin, possibly within the inner mesaxon.

To confirm the unexpected observation of peroxisomes in non-compacted myelin also for the CNS, we combined immuno-gold labeling with electron microscopy. Focussing on the corpus callosum and the spinal cord, we stained for PMP70 (followed by binding to protein A linked to 15 nm colloidal gold) or catalase (10 nm colloidal gold). Indeed, we found catalase and PMP70-positive, single-membrane vesicles in the inner mesaxon and, more frequently, in the outer mesaxon of myelin (Fig. 2C–E). Here, out of 40 documented immuno-labeled peroxisomes found in cross-sections, none was located inside an axon (data not shown). In contrast to the widely studied liver peroxisomes (up to 1 μm in diameter), the myelin-associated peroxisomes were small and variable in size (30–150 nm).

3.3. Peroxisomes enter the myelin compartment after myelination

Myelin-associated peroxisomes are sufficiently small to reach non-compacted compartments by passive movement, and we hypothesized that they are targeted to (or restricted from) specific regions of the myelin sheath. Indeed, by double-immunolabeling of teased fibers with PEX14 (or PMP70 and Catalase) and MAG, peroxisomes were less abundant in Schmidt-Lanterman incisures than in the paranodal region (Fig. 3A and B).

It is theoretically possible that myelin-associated peroxisomes are merely stable "leftover" organelles, wrapped up during myelination. Alternatively, they are transported later into myelin. To address this question, we prepared teased nerve fibers from mice at age P5 and P10. Interestingly, at this earlier developmental stage (but clearly after the onset of myelination) paranodes showed no or only very few PEX14-positive puncta (Fig. 3C). This suggests that peroxisomes enter this compartment after myelination, most likely by means of a tubulin-associated organelle transport.

3.4. Paranodal swellings in mice lacking functional peroxisomes in Schwann cells

To study the functional relevance of peroxisomes in myelinated fibers, we analyzed the PNS of CNP-Cre*Pex5 conditional mouse mutants, originally developed as a 'phenocopy' model of cerebral

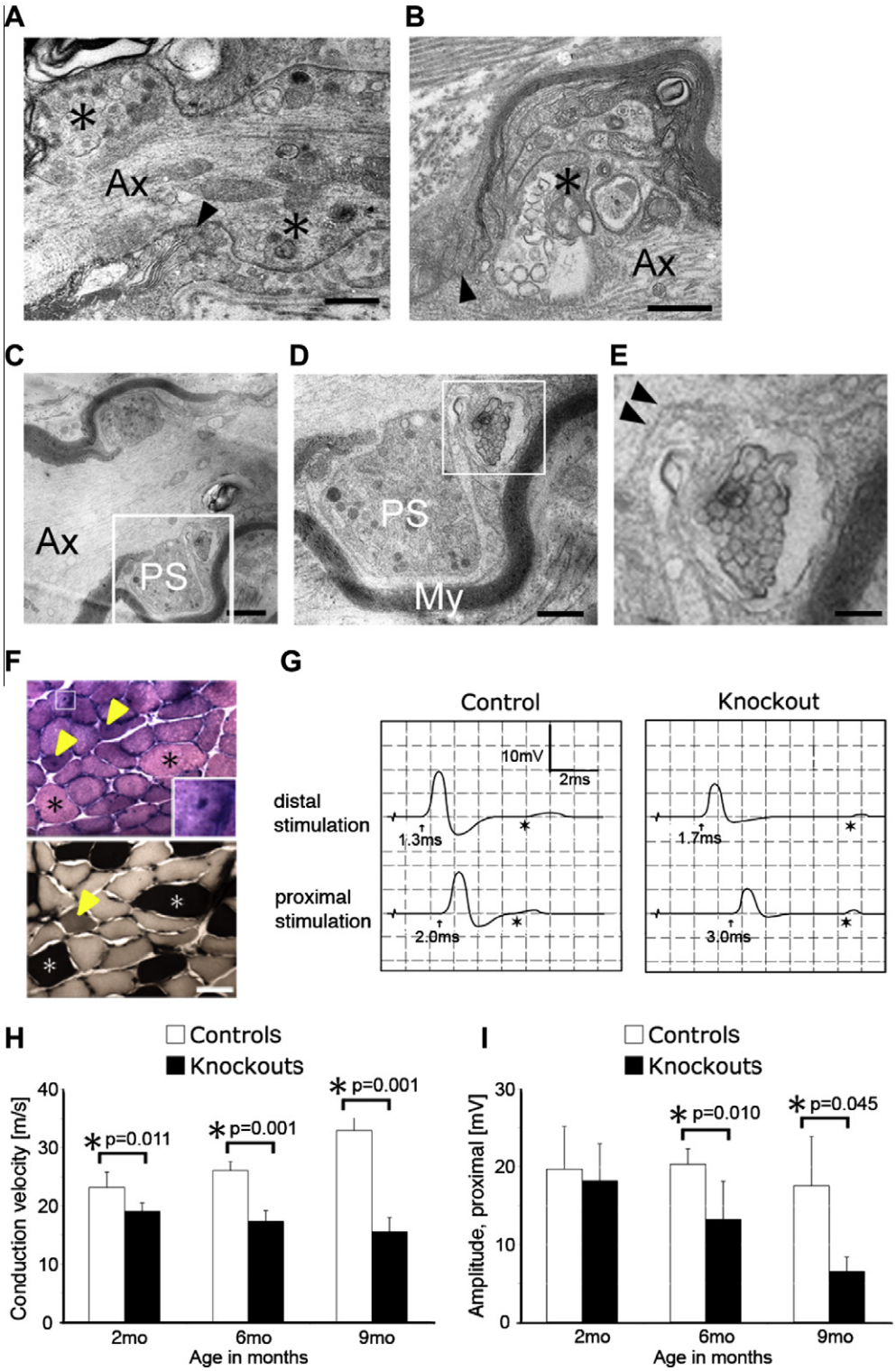

Fig. 4. A peripheral neuropathy in conditional Pex5 mutant mice. (A) Axonal abnormalities close to the node of Ranvier in a teased fiber preparation from 2 months old mice, long before the onset of disease. Note vesicular accumulations and axonal protuberances (asterisces). Ax, axon. Arrowhead, paranodal loops. Scale bar 600 nm. (B) Paranodal swelling with vesicular inclusions and multivesicular bodies (asterisk). Arrowhead, paranodal loops. Scale bar 500 nm. (C) Paranodal swellings leading to a cuff-like structure are frequently seen at 12 months of age. Scale bar 1 μm. PS, paranodal swelling; Ax, axon. (D) Magnified inset of (C). Note vesicles of different electron-density, possibly lipid loaden. PS, paranodal swelling; My, myelin. Scale bar 500 nm. (E) Magnified inset of (D). Note the continuity (arrowheads) of the vesicular assembly with the paranodal swelling (PS in panel D) and thus with the Schwann cell. Scale bar 250 nm. (F) Pathology of the soleus muscle in mutants at 9 months. Consecutive sections were analyzed by H&E staining (top) and ATPase histochemistry at pH 4.3 (bottom) revealing a checkerboard distribution of light (type II) and dark (type I) muscle fibers. Hypertrophic fibers (asterisces), intermediate stained fibers (arrowhead, bottom), and fibers with centrally located nuclei (arrowheads, top) are indicative of muscle fiber degeneration and regeneration. Scale bar 25 μm. (G) Representative sciatic nerve recordings in a 9 months old control (left) and mutant mouse (right) after distal (top) and proximal (bottom) stimulation. The mutant response is characterized by reduced nerve conduction velocity, reduced amplitude, and a delayed F-wave (asterisk). (H) Quantification of nerve conduction velocity at 2, 6 and 9 months of age. A significant difference (−18%) between mutants and controls is detectable at 2 months, and progressively enhanced at 6 months (−33%) and 9 months (−53%) (mean ± S.D.; $n \geqslant 3$). (I) Quantification of electrophysiological response amplitudes after proximal stimulation of the sciatic nerve in mutants and controls. A significant difference is detected at 6 months and 9 months in PEX5 mutant mice (mean ± S.D.; $n \geqslant 3$).

X-linked ALD [14]. In contrast to the severe inflammatory demyelination in the CNS of these mice, which is morphologically complex, the changes of peripheral nerves appeared minor by gross inspection. We therefore turned to teased fiber preparations from sciatic nerves of mutants and controls, aged 2, 6 and 12 months (Fig. 4A–E, Suppl. Fig. 3 and not shown). Paranodal regions showed vacuolizations and delamination of myelin membranes. Although common artifacts in electron microscopy of myelin (not shown), these features were more frequent (81%) in 2 months old mutants than in controls (28%), and constitute therefore an 'informative' phenotype. We also observed secondary axonal changes in nodal regions, such as protuberances that resembled early axonal swellings (Fig. 4A). At 6 months, we noticed "paranodal swellings" (Fig. 4B–D), a novel pathological feature that affected a significant fraction of paranodes at 1 year. Typically, at least one paranodal loop was abnormally extended and filled with vesicles of different sizes and different electron density (Fig. 4B–E), morphologically reminiscent of axonal swellings in CNS myelin diseases [22]. In some cases, it was not even possible to clarify whether these swellings were of axonal or glial origin, but paranodal swellings could often be defined by their morphological continuity with Schwann cell cytoplasm (Fig. 4C–E).

In older mutants, the clinical phenotype included a peripheral neuropathy with muscle weakness. In the m. soleus, we found hypertrophic fibers, intermediate ATPase stainings of slow twitch fibers, and fibers with centrally located nuclei, collectively indicating muscle fiber degeneration and regeneration (Fig. 4F), presumably secondary to axon loss.

To determine possible impairments of nerve conduction, we performed electrophysiological recordings (Fig. 4G–I). Indeed, 9 months old mice exhibited slower motor nerve conduction velocity (NCV) and reduced current amplitudes after proximal and distal stimulation (Fig. 4G). Importantly, peripheral NCV was already significantly reduced in 2 months old mutants compared to controls, but progressed further at older ages (Fig. 4H). In contrast, the amplitude of these responses was only decreased in nerves from 6 and 9 months old mutant mice. Although we have no morphological evidence for motoneuron death in adult spinal cord (Suppl. Fig. 3), it cannot be excluded that CNS-derived defects in this mutant contribute to a reduced nerve conduction velocity.

4. Discussion

While peroxisomes have been described in axons [20] and oligodendrocytes [12,13], we made the unexpected observation that most peroxisomes in long fiber tracts of CNS white matter and in peripheral nerves are of glial origin, and virtually absent from axons. Because of their small size (30 nm is far below the spatial resolution of fluorescence microscopy) and their ability to form clusters, the quantitation of peroxisomes is difficult. Many of the peroxisomes are physically associated with the myelin sheath itself and are small in size. At least in the PNS, peroxisomes emerge in distal glial compartments after myelination has begun, suggesting that they are not captured during myelination but transported. Indeed, peroxisomes were not required for myelination. Paranodes, in which peroxisomes are most abundant, are sites of axon–glial communication and required for axonal integrity after myelination [23]. PEX5 mutant mice develop a novel peripheral neuropathy at an older age, associated with axonal dysfunction and muscle dystrophy.

Our findings are relevant for several diseases associated with peroxisomal dysfunction. For example in X-linked adrenomyeloneuropathy (AMN), the progressive axonopathy of long spinal tracts was thought to reflect a peroxisomal failure in the affected spinal cord axons [24]. Our finding that peroxisomes in the white matter are associated with oligodendrocytes and myelin rather than axonal projections strongly supports the model that AMN is a primary glial dysfunction with secondary axonal involvement that is responsible for progressive clinical disability.

The paranodal swellings described in peripheral nerves of Pex5 mutant mice are, to our knowledge, a novel pathological feature and differ from previously described paranodal swellings/tomacula, such as in diabetic neuropathy [25]. However, they resemble previously observed Schwann cell processes in normal nerve fibers [26,27] thought to phagocytose and internalize degenerated axonal organelles and vesicular material, especially in the paranodal region. It is possible that Schwann cell peroxisomes are involved in the fatty acid oxidation following myelin membrane degradation in the endosomal–lysosomal compartment of the paranode, and that this process stalls in conditional Pex5 mutant mice. Moreover, we note that a targeted disruption of the peroxisomal dihydroxyacetonephosphate acyltransferase (DAPAT) gene causes paranodal abnormalities [28] that could precede and be related to those reported in the present study.

Alternatively, paranodal swellings are secondary to a perturbed intracellular transport within the distal cytosolic Schwann cell compartments, similar to a perturbed axonal transport [29]. We note that Cnp1 mutant mice, which develop secondary axonal degeneration in CNS fiber tracts, exhibit similar swellings underneath non-compact myelin, but predominantly originating at the inner mesaxon [3].

Acknowledgements

We thank J. Barth, A. Fahrenholz, and T. Ruhwedel for technical support and members of the Nave lab for discussions. This work was supported by grants from EU-FP6 (X-ALD and PEROXISOME), DFG (SFB/TR43) and Oliver's Army.

Appendix A. Supplementary data

Supplementary data associated with this article can be found, in the online version, at doi:10.1016/j.febslet.2011.05.032.

References

[1] Lazzarini, R.A. (2004) Myelin Biology and Disorders, Elsevier Academic Press.
[2] Griffiths, I. et al. (1998) Axonal swellings and degeneration in mice lacking the major proteolipid of myelin. Science 280, 1610–1613.
[3] Lappe-Siefke, C., Goebbels, S., Gravel, M., Nicksch, E., Lee, J., Braun, P.E., Griffiths, I.R. and Nave, K.-A. (2003) Disruption of Cnp1 uncouples oligodendroglial functions in axonal support and myelination. Nat. Genet. 33, 366–374.
[4] Yin, X., Baek, R.C., Kirschner, D.A., Peterson, A., Fujii, Y., Nave, K.-A., Macklin, W.B. and Trapp, B.D. (2006) Evolution of a neuroprotective function of central nervous system myelin. J. Cell Biol. 172, 469–478.
[5] Suter, U. and Scherer, S.S. (2003) Disease mechanisms in inherited neuropathies. Nat. Rev. Neurosci. 4, 714–726.
[6] Nave, K.-A., Sereda, M.W. and Ehrenreich, H. (2007) Mechanisms of disease: inherited demyelinating neuropathies—from basic to clinical research. Nat. Clin. Pract. Neurol. 3, 453–464.
[7] Nave, K.-A. (2010) Myelination and the trophic support of long axons. Nat. Rev. Neurosci. 11, 275–283.
[8] Wanders, R.J.A. and Waterham, H.R. (2006) Biochemistry of mammalian peroxisomes revisited. Annu. Rev. Biochem. 75, 295–332.
[9] Bonekamp, N., Völkl, A., Fahimi, H. and Schrader, M. (2009) Reactive oxygen species and peroxisomes: struggling for balance. Biofactors 35, 346–355.
[10] Stadelmann-Ingrand, S., Pontcharraud, R. and Fauconneau, B. (2004) Evidence for the reactivity of fatty aldehydes released from oxidized plasmalogens with phosphatidylethanolamine to form Schiff base adducts in rat brain homogenates. Chem. Phys. Lipids 131, 93–105.
[11] Steinberg, S.J., Dodt, G., Raymond, G.V., Braverman, N.E., Moser, A.B. and Moser, H.W. (2006) Peroxisome biogenesis disorders. Biochim. Biophys. Acta 1763, 1733–1748.
[12] Mckenna, O., Arnold, G. and Holtzman, E. (1976) Microperoxisome distribution in the central nervous system of the rat. Brain Res. 117, 181–194.
[13] Ahlemeyer, B., Neubert, I., Kovacs, W.J. and Baumgart-Vogt, E. (2007) Differential expression of peroxisomal matrix and membrane proteins during postnatal development of mouse brain. J. Comp. Neurol. 505, 1–17.

[14] Kassmann, C.M. et al. (2007) Axonal loss and neuroinflammation caused by peroxisome-deficient oligodendrocytes. Nat. Genet. 39, 969–976.
[15] Hulshagen, L. et al. (2008) Absence of functional peroxisomes from mouse CNS causes dysmyelination and axon degeneration. J. Neurosci. 28, 4015–4027.
[16] Bottelbergs, A., Verheijden, S., Hulshagen, L., Gutmann, D.H., Goebbels, S., Nave, K.-A., Kassmann, C. and Baes, M. (2010) Axonal integrity in the absence of functional peroxisomes from projection neurons and astrocytes. Glia 58, 1532–1543.
[17] Trotter, J. and Schachner, M. (1989) Cells positive for the O4 surface antigen isolated by cell sorting are able to differentiate into astrocytes or oligodendrocytes. Brain Res. Dev. Brain Res. 46, 115–122.
[18] Jung, M., Sommer, I., Schachner, M. and Nave, K.A. (1996) Monoclonal antibody O10 defines a conformationally sensitive cell-surface epitope of proteolipid protein (PLP): evidence that PLP misfolding underlies dysmyelination in mutant mice. J. Neurosci. 16, 7920–7929.
[19] Werner, H.B. et al. (2007) Proteolipid protein is required for transport of sirtuin 2 into CNS myelin. J. Neurosci. 27, 7717–7730.
[20] Bradke, F. and Dotti, C.G. (1997) Neuronal polarity: vectorial cytoplasmic flow precedes axon formation. Neuron 19, 1175–1186.
[21] Hoepfner, D., Schildknegt, D., Braakman, I., Philippsen, P. and Tabak, H.F. (2005) Contribution of the endoplasmic reticulum to peroxisome formation. Cell 122, 85–95.
[22] Nave, K.-A. and Trapp, B.D. (2008) Axon–glial signaling and the glial support of axon function. Annu. Rev. Neurosci. 31, 535–561.
[23] Sousa, A. and Bhat, M. (2007) Cytoskeletal transition at the paranodes: the Achilles' heel of myelinated axons. Neuron Glia Biol. 3, 169–178.
[24] Powers, J.M., DeCiero, D.P., Ito, M., Moser, A.B. and Moser, H.W. (2000) Adrenomyeloneuropathy: a neuropathologic review featuring its noninflammatory myelopathy. J. Neuropathol. Exp. Neurol. 59, 89–102.
[25] Thomas, P.K. et al. (1996) Paranodal structure in diabetic sensory polyneuropathy. Acta Neuropathol. 92, 614–620.
[26] Spencer, P.S. and Thomas, P.K. (1974) Ultrastructural studies of the dying-back process. II. The sequestration and removal by Schwann cells and oligodendrocytes of organelles from normal and diseases axons. J. Neurocytol. 3, 763–783.
[27] Gatzinsky, K.P., Persson, G.H. and Berthold, C.H. (1997) Removal of retrogradely transported material from rat lumbosacral alpha-motor axons by paranodal axon–Schwann cell networks. Glia 20, 115–126.
[28] Teigler, A., Komljenovic, D., Draguhn, A., Gorgas, K. and Just, W.W. (2009) Defects in myelination, paranode organization and Purkinje cell innervation in the ether lipid-deficient mouse cerebellum. Hum. Mol. Genet. 18, 1897–1908.
[29] Edgar, J.M. et al. (2004) Oligodendroglial modulation of fast axonal transport in a mouse model of hereditary spastic paraplegia. J. Cell Biol. 166, 121–131.